MoS2-assisted growth of highly-oriented AlN thin films by low-temperature van der Waals epitaxy

J. Patouillard, M. Bernard, S. Cadot, R. Gassilloud, N. Bernier, A. Grenier, A. Mantoux, Elisabeth Blanquet, F. Martin, C. Raynaud, et al.

Journal of Vacuum Science and Technology A

LETTER | JULY 10 2024

MoS_2-assisted growth of highly-oriented AlN thin films by low-temperature van der Waals epitaxy

J. Patouillard ; M. Bernard; S. Cadot ; R. Gassilloud ; N. Bernier ; A. Grenier; A. Mantoux ; E. Blanquet; F. Martin; C. Raynaud; F. Gianesello

J. Vac. Sci. Technol. A 42, 050401 (2024)
https://doi.org/10.1116/6.0003652

JVST A
Journal of Vacuum Science & Technology A

LETTER

pubs.aip.org/avs/jva

MoS_2-assisted growth of highly-oriented AlN thin films by low-temperature van der Waals epitaxy

Cite as: J. Vac. Sci. Technol. A **42**, 050401 (2024); doi: 10.1116/6.0003652
Submitted: 27 March 2024 · Accepted: 14 June 2024 ·
Published Online: 10 July 2024

J. Patouillard,[1,2,3,a)] M. Bernard,[1] S. Cadot,[1] R. Gassilloud,[1] N. Bernier,[1] A. Grenier,[1] A. Mantoux,[2] E. Blanquet,[2] F. Martin,[1] C. Raynaud,[1] and F. Gianesello[3]

AFFILIATIONS

[1]Université Grenoble Alpes, CEA, LETI, F-38000 Grenoble, France
[2]Univ. Grenoble Alpes CNRS, Grenoble INP, SIMaP, 38000 Grenoble, France
[3]STMicroelectronics, 850 rue Jean Monnet, F-38926 Crolles, France

[a)]**Author to whom correspondence should be addressed:** julien.patouillard2@cea.fr

ABSTRACT

Aluminum nitride (AlN) is a wide bandgap material used in acoustic devices, piezo- micro-electromechanical system and is promising for other electronic applications. However, for most applications, the AlN crystalline quality obtained by PVD or MOCVD is insufficient, and suitable growth substrates providing an adapted lattice match and coefficient of thermal expansion are limited. Alternatively, monocrystalline AlN wafers are not yet available in 200/300 mm sizes and suffer from high costs and quality issues. Here, we propose a novel approach involving a two-dimensional transition metal dichalcogenide (TMD) material as a seed layer, which displays an excellent lattice matching with AlN (>98%) allowing a strong enhancement in the c axis texture of sputtered AlN layers on Si(100)/SiO_2 thermal oxide (500 nm) substrates. We have successfully demonstrated an eightfold improvement of the AlN (002) rocking curve compared to reference samples grown on thermal SiO_2, thus providing a relevant and cost-effective process for the large-scale deployment of high-quality III-N materials on silicon-based substrates.

I. INTRODUCTION

AlN is a wide bandgap (6.2 eV)[1] and piezoelectric material, which crystallizes in a hexagonal wurtzite structure. It shows its highest piezoelectric response along the c axis ($d_{33} = 5.53$ pm V^{-1}). Hence, c axis textured AlN is widely used as a piezoelectric layer in many applications such as surface or bulk acoustic wave resonators (SAW and BAW), micro-electromechanical systems (MEMSs) and others. Its deposition process is well-known and appears to be very reproducible, using either N_2-based reactive sputtering (with Al-target) or MOCVD processes on epitaxial substrates. It also exhibits a relatively large electromechanical coupling coefficient $k^2_{eff} \approx 7\%$ (Ref. 2) when integrated in resonators. However, the crystal quality of the sputtered AlN layers remains limited. The FWHM of the (002) rocking curve (RC), used to assess the texture of the AlN film, is typically higher than 1° on silicon-based substrates after a direct sputtered AlN growth.

To overcome this issue and enhance AlN texture (RC below 1°), two trends are commonly explored. First, substrates displaying a good in-plane lattice match with AlN sputtered layers such as sapphire[3,4] or silicon carbide (SiC)[5,6] can be used. However, high cost and limited wafer size of these substrates limit large-scale integration of high-quality AlN thin films. Second, another straightforward solution to grow AlN is to investigate high-temperature deposition method such as metal organic chemical vapor deposition (MOCVD).[7–9] However, due to the large lattice mismatch between AlN and silicon resulting in high dislocation density, it requires monocrystalline sapphire or silicon carbide (SiC) substrates at high growth temperatures (≈1000 °C). It enables to achieve high-quality AlN thin films but at extreme costs due to the expensive sapphire and SiC substrates and high thermal budget. Therefore, no easy current solution seems to exist to achieve highly c axis textured AlN thin films by direct growth.

In recent years, new innovative approaches have emerged to grow high-quality AlN layers. Indeed, a few studies reported the interest of a thin Al predeposition layer before AlN sputtering on (111)-oriented Si substrates, enabling to achieve single-crystalline AlN layer[10] and an AlN (002) RC close to 0.65°.[11] In addition, the emergence of two-dimensional (2D) materials and particularly 2D-transition metal dichalcogenides (2D-TMDs) also appeared as

a suitable solution to grow III-N layers.[12,13] These 2D materials can be deposited on a wide range of substrates[14] and could be a potential straightforward solution to deposit highly c axis textured AlN films independently with the substrate. Among 2D-TMDs, MoS_2 is one of the most widely studied materials due to its availability and long-term stability under aerobic conditions.[15,16] MoS_2 has a natural layered structure where each layer consists of a molybdenum layer sandwiched between two sulfur layers in a trigonal prismatic arrangement. The Mo–S bonds are strongly covalent, while individual S–Mo–S layers are only coupled by weak van der Waals (vdW) interactions, resulting in an easy cleavage of the layers and possible isolation of a single (2D) MoS_2 layer.[17,18]

Interest of TMDs and especially MoS_2 and WS_2 in AlN texturing is based on their crystal structure compatibility. Both TMDs show hexagonal AlN-like structures and present a very small lattice mismatch with AlN ($\Delta a = 1.6\%$). The first evaluation of TMDs as a growth template for crystalline AlN was conducted in 1996 by Chung and Ohuchi.[12] More recently, further studies were published with AlN grown by helicon sputtering[19,20] or MOCVD[21] on TMDs deposited by CVD methods. In the present work, we focus on the enhancement of aluminum nitride (AlN) crystal quality and, in particular, its c axis orientation using an ALD-grown MoS_2 thin film as a template. AlN is deposited by low-temperature reactive sputtering without substrate biasing in order to preserve the integrity of the MoS_2 template.

II. EXPERIMENT

A. Fabrication process

MoS_2 samples were deposited by ALD on a $Si(100)/SiO_2$ (500 nm) substrate at 90 °C using $Mo(NMe_2)_4$ and 1,2-ethanedithiol as precursors.[16] Crystallization annealing under a N_2 flow ($2\,l\,min^{-1}$) was subsequently performed at 900 °C for 30 s under atmospheric pressure. The number of ALD cycles is adjusted in order to obtain a thickness of three MoS_2 monolayers, which are perfectly 001-oriented after annealing.

Then, AlN thin films with a thickness of 100 nm were deposited by reactive sputtering in a SPTS (Trikon) Sigma fxP 200 mm magnetron PVD reactor located in CEA-LETI. The deposition parameters were initially adjusted to achieve the best texture of the AlN films on Si (100)/SiO_2 (500 nm)/MoS_2 (3 monolayers) wafers. The temperature was set to 350 °C with a standard target power of 2 kW. The argon and nitrogen flow rates for the plasma were set to 10 and 50 SCCM, respectively. The deposition was performed without bias in order to prevent any degradation of the MoS_2 seed layer.

B. Characterizations

Raman spectra were collected in the backscattering geometry using a Renishaw In-Via spectrometer equipped with a Peltier cooled charge coupled device detector. The light was focused onto the sample surface using a ×100 (0.85 numerical aperture) short working objective lens (0.27 mm). The resulting spot diameter was around 0.7 μm. A 532 nm wavelength laser diode was used as light source with a typical laser power of 1 mW. Raman spectra experimental line shapes were fitted with Gaussian–Lorentzian components on WIRE software.

The XPS spectra were recorded with a PHI 5000 VersaProbe II spectrometer (Physical Electronics) using monochromatic Al K_α radiation (1486.6 eV) and with an overall energy resolution of 0.6 eV (with silver as a reference). The analysis angle was set at 45°. The experimental line shapes were fitted with Gaussian–Lorentzian [G-L (70-30)] components on CASAXPS software.

For TEM analysis, the sample was prepared by Ga^+ focused ion beam (FIB) milling. The thin foil was observed in an STEM mode at 200 kV using a convergence semiangle of ≈18 mrad for the incident electron probe in a probe-corrected ThermoFisher Titan Themis microscope. Gun lens and spot size values were selected to provide a probe current of approximately 20 pA. We paid attention to verify that there was no electron beam induced damage by comparing STEM images before and after each STEM acquisition.

XRD out-of-plane measurements (Rocking curve, 2θ/θ scans and XRR) have been performed using Panalytical® Xpert 4 circles goniometer equipped with a Cu-$K_{\alpha 1}$ anode ($\lambda_{Cu} = 1.5406$ Å) as source. The beam is monochromatized and collimated with a multilayer curved mirror and a parallel plate collimator is mounted in the diffracted beam path.

III. RESULTS

Structural integrity of the 2D-MoS_2 layer after AlN deposition was assessed by Raman spectroscopy before and after deposition. It is worth noting that at the working wavelength (532 nm), AlN is highly transparent (transmittance close to 80%–90%).[22,23] First, and as presented in Fig. 1, no significant degradation of the MoS_2 Raman signal is observed after AlN deposition. We still observe the presence of E^1_{2g} and A_{1g} modes, at reduced intensities since MoS_2 is capped with 100 nm thick AlN. Second, after AlN deposition, a slight redshift is visible on both vibration modes. In fact, E^1_{2g} and A_{1g} modes are located at $382.6 \pm 0.2\,cm^{-1}$ and $407.9 \pm 0.1\,cm^{-1}$

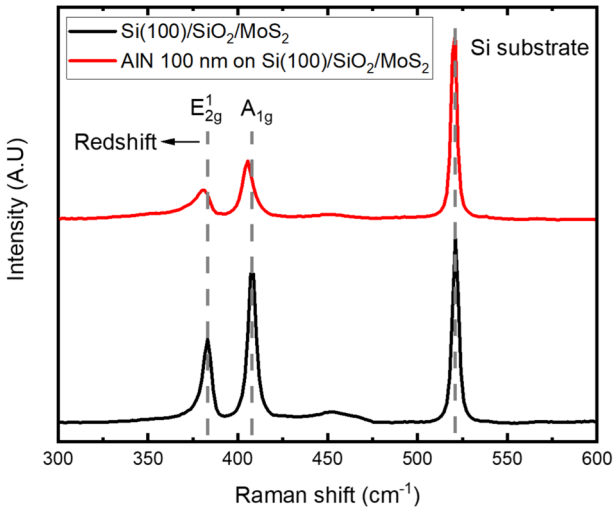

FIG. 1. Raman spectrum of the $Si(100)/SiO_2$ (500 nm)/MoS_2 sample before (bottom) and after (top) AlN deposition (100 nm).

before AlN deposition, and $379.2 \pm 0.4\ cm^{-1}$ and $405.5 \pm 0.1\ cm^{-1}$ after deposition, respectively. This redshift could be related to the in-plane tensile stress in MoS_2 induced by the deposition of the AlN layer. Finally, an increase in the FWHM of both MoS_2 modes is observed after AlN deposition (4.7 ± 0.2–$8.6 \pm 0.3\ cm^{-1}$ for E^1_{2g} and 5.6 ± 0.1–$7.3 \pm 0.2\ cm^{-1}$ for A_{1g}). These results, associated with a decrease of the overall signal intensity after AlN deposition, emphasize a slight deterioration of the MoS_2 layer after the AlN reactive sputtering process.

To assess the texture of the AlN on Si(100)/SiO_2 500 nm/MoS_2 3 monolayers (ML) film, a ω-scan XRD measurement of AlN (002) planes has been performed and compared with a reference AlN layer on a MoS_2-free substrate [Si(100)/SiO_2 500 nm]. As can be seen from Fig. 2, the AlN (002) RC is strongly enhanced by the presence of the MoS_2 seed layer (RC ≈ 0.5° with MoS_2 versus 4.0° without MoS_2).

Finally, the crystallinity of the MoS_2 layer before and after AlN deposition has also been investigated by STEM studies. Cross-sectional images of AlN/MoS_2 stacks are shown in Figs. 3(a) and 4(a) and compared with the AlN layer deposited on SiO_2 using the same conditions [see Figs. 3(b) and 4(b)].

In Fig. 3(a), the polycrystalline AlN film displays a typical columnar structure with 15–20 nm-width grains. This size seems to correspond to the lateral MoS_2 domain size, as reported in the literature for MoS_2 layers obtained through a similar process and shown in Fig. 3(c) (ALD deposition at low temperatures followed by crystallization annealing at 800 °C).[24] Hence, we can conclude that the shape and orientation of MoS_2 grains is transferred to the AlN layer thanks to a van der Waals epitaxy mechanism.[25]

In Fig. 3(b), the AlN grains size on SiO_2 seems slightly lower than those observed on 2D-MoS_2. The typical columnar growth remains visible but less marked, suggesting a lower c axis orientation. In addition, the AlN top surface displays a higher roughness on SiO_2 compared to the MoS_2 substrate, further suggesting less disordered AlN growth on MoS_2. Figure 4(a) shows an atomic resolution image of the MoS_2/AlN interface centered in a grain. We clearly observe a clean and sharp interface without any visible damage in the MoS_2 structure and, within the limit of the image resolution, highlighting an excellent lattice arrangement between MoS_2 and AlN crystals. However, these observations are not aligned with Raman results presented in Fig. 1 which show an increase in FWHM of E^1_{2g} and A_{1g} MoS_2 Raman modes and suggest MoS_2 degradation. These differences could be explained by a scale effect: the proposed TEM image is an atomic scale measurement while Raman is a macro-measurement (laser spot size around 0.7 μm). Finally the atomic-scale structure of AlN is not visible in

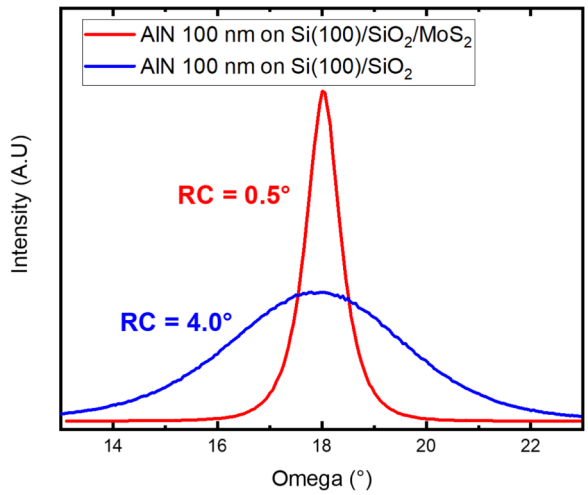

FIG. 2. XRD spectra [AlN (002) omega scan] of a 100 nm-thick AlN layer deposited on MoS_2 (red line) vs SiO_2 (blue line) substrates.

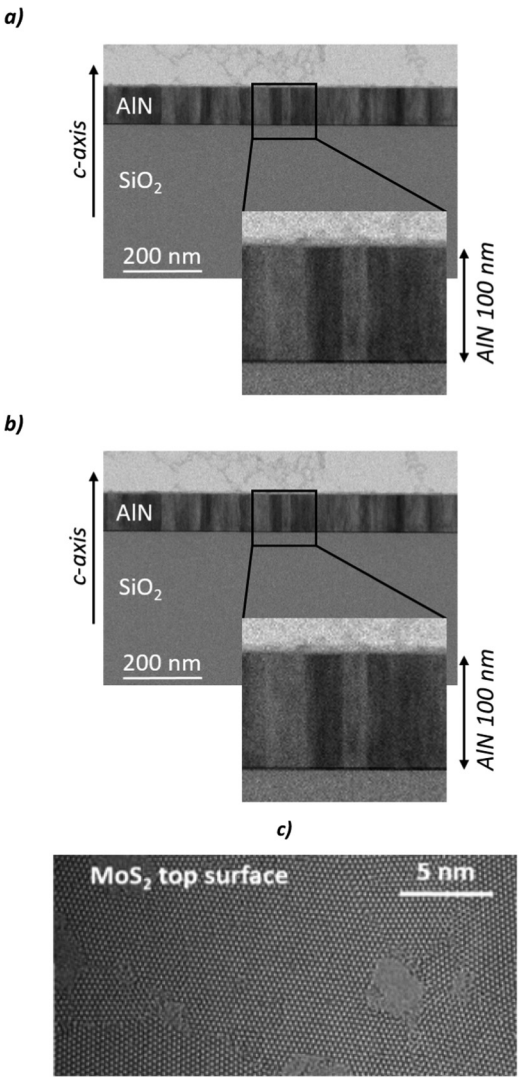

FIG. 3. Cross-sectional STEM of the 100 nm AlN PVD deposited on (a) Si (100)/SiO_2 (500 nm)/MoS_2 (3 monolayers); (b) Si (100)/SiO_2 (500 nm). (c) represents a TEM top view of the MoS_2 crystalline domains size after an annealing at 800 °C under Ar.

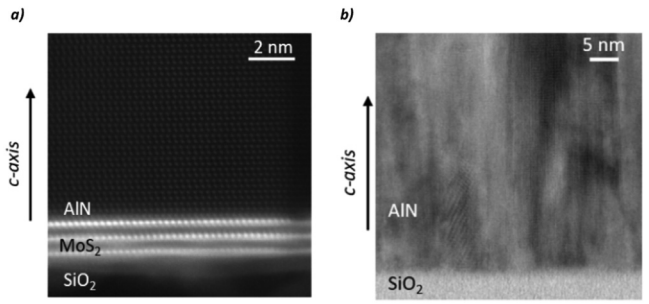

FIG. 4. Cross-sectional STEM at an atomic resolution of the 100 nm AlN PVD deposited on (a) MoS_2 (3 monolayers); (b) SiO_2 (500 nm).

Fig. 4(b), confirming a much lower crystallinity of the AlN layer on the amorphous SiO_2 substrate.

IV. DISCUSSION

In order to limit the damages on MoS_2 during AlN deposition, reactive sputtering was performed without biasing the substrate. However, the formation of a sharp and defect-free AlN/MoS_2 interface was rather surprising. By principle, the PVD deposition technique relies on the atomic sputtering of a target, where sputtered elements can gain sufficient kinetic energy to induce an implantation effect on the substrate at least through the first nanometers. This is particularly true under the sputtering conditions used for this study (2 kW). As the MoS_2 structure is expected to be quite sensitive to such ballistic effects due to the low energy of the Mo–S bond (compared to most metal oxides), we would expect a strong degradation of the MoS_2 seed layer. However, as shown in Fig. 4(a), the crystalline structure of MoS_2 is preserved and only local defects are revealed by Raman spectroscopy after AlN deposition (increase in FWHM of E^1_{2g} and A_{1g} MoS_2 Raman modes, see Fig. 1).

Overall, these results demonstrate the unique capability of the MoS_2 layer to offer a highly c axis oriented and flexible substrate which is able to accommodate the mismatch with AlN and the stress/strain induced by the AlN layer through different mechanisms (dislocations, twisting, buckling oscillations, etc.). Hence, the use of layered TMDs as a seed layer prevents the propagation of defects into the AlN layer, as it typically occurs when rigid epitaxial substrates such as SiC or sapphire are used. The strong improvement in the AlN texture [RC FWHM value of 0.5° on MoS_2 versus 4° on SiO_2 and 2.3° on Si (111)[26]] relies on the fact that during the first stages of the AlN growth, the Al and N atoms are relatively well aligned with the S and Mo atoms of the MoS_2 crystals, which also provide an atomically flat and c-oriented surface, as can be seen in Fig. 4(a). As our ALD-grown MoS_2 displays relatively small domains (typically 10–20 nm wide), we could expect even better results using a CVD-grown MoS_2 as reported in the literature.[19] In fact, the synthesis of MoS_2 by CVD technique leads to large crystallite sizes up to a few μm, which would drastically reduce the density of local defects and grain boundaries, and therefore decrease the number of non-c-aligned AlN nuclei. Increasing the AlN thickness would also further improve the c axis texture (as typically observed for most materials having a columnar growth).[27]

V. CONCLUSIONS

In this work, highly c axis textured AlN films with an AlN (002) RC value of 0.5° (for a 100 nm-thick film) were obtained, thanks to a MoS_2 seed layer providing an efficient van der Waals epitaxial growth, and a finely tuned AlN process preventing destructuring of the seed layer. This represents a substantial improvement of the RC FWHM value compared to a similar AlN layer grown on an amorphous SiO_2 substrate (RC FWHM = 4°) or literature data reported on Si (111) substrates (RC FWHM = 2.3°). Such a strategy demonstrated its unique capacity to provide a cost-effective epitaxial substrate that can handle and relax the stress generated by the lattice mismatch, therefore preventing the formation of dislocations in the target AlN material. Eventually, this approach could be extended to other III-N materials such as gallium nitride, using large-grain CVD-grown MoS_2 or WS_2 seed layers that will ensure the formation of unprecedented quality III-N materials. Besides, the poorly adhesive TMD-based seed layer could also serve as a detachment layer in order to transfer the III-N layer on any kind of planarized substrates.

ACKNOWLEDGMENTS

The authors would like to thank Audrey Jannaud and Hugo Dansas for the FIB-STEM sample preparation and Hanako Okuno for the top surface MoS_2 STEM image. Part of this work was performed at the Platform for Nanocharacterization of the CEA Grenoble, MINATEC Campus, with support from the French Recherche Technologique de Base programme.

AUTHOR DECLARATIONS

Conflict of Interest

The authors have no conflicts to disclose.

Author Contributions

J. Patouillard: Investigation (lead); Methodology (equal); Writing – original draft (lead); Writing – review & editing (lead). **M. Bernard:** Investigation (equal); Methodology (equal); Supervision (equal). **S. Cadot:** Supervision (equal); Validation (equal); Writing – review & editing (equal). **R. Gassilloud:** Supervision (equal); Writing – review & editing (lead). **N. Bernier:** Formal analysis (equal); Validation (supporting); Writing – review & editing (equal). **A. Grenier:** Formal analysis (equal); Validation (supporting); Writing – review & editing (equal). **A. Mantoux:** Methodology (equal); Supervision (equal); Validation (equal); Writing – review & editing (equal). **E. Blanquet:** Methodology (equal); Supervision (equal); Validation (equal); Writing – review & editing (equal). **F. Martin:** Methodology (equal); Validation (equal). **C. Raynaud:** Supervision (equal). **F. Gianesello:** Supervision (equal).

DATA AVAILABILITY

The data that support the findings of this study are available within the article.

REFERENCES

[1]H. Yamashita, K. Fukui, S. Misawa, and S. Yoshida, J. Appl. Phys. **50**, 896 (1979).
[2]P. Muralt, "AlN thin film processing and basic properties," in *Piezoelectric MEMS Resonance*, edited by H. Bhugra and G. Piazza (Springer International Publishing, Cham, 2017), pp. 3–37.
[3]T. Kumada, M. Ohtsuka, K. Takada, and H. Fukuyama, Phys. Status Solidi (C) **9**, 515 (2012).
[4]H. Liu and W. Guo, Semicond. Sci. Technol. **38**, 015020 (2023).
[5]W. Z. Wang, Y. Ruan, and Z. You, "AlN/6H-SiC SAW resonator for high temperature wireless SAW sensor," in *2017 19th International Conference on Solid-State Sensors and Actuators Microsystem Transducers*, Kaohsiung, Taiwan, 18-22 June 2017 (IEEE, Kaohsiung, 2017), pp. 942–945.
[6]K. Uesugi, Y. Hayashi, K. Shojiki, S. Xiao, K. Nagamatsu, H. Yoshida, and H. Miyake, J. Cryst. Growth **510**, 13 (2019).
[7]Z. Chen, S. Newman, D. Brown, R. Chung, S. Keller, U. K. Mishra, S. P. Denbaars, and S. Nakamura, Appl. Phys. Lett. **93**, 191906 (2008).
[8]Y. Guo, Y. Fang, J. Yin, Z. Zhang, B. Wang, J. Li, W. Lu, and Z. Feng, J. Cryst. Growth **464**, 119 (2017).
[9]I. Demir, H. Li, Y. Robin, R. McClintock, S. Elagoz, and M. Razeghi, J. Phys. Appl. Phys. **51**, 085104 (2018).
[10]I.-S. Shin, J. Kim, D. Lee, D. Kim, Y. Park, and E. Yoon, Jpn. J. Appl. Phys. **57**, 060306 (2018).
[11]A. Dadgar, F. Hörich, R. Borgmann, J. Bläsing, G. Schmidt, P. Veit, J. Christen, and A. Strittmatter, Phys. Status Solidi (A) **220**, 2200609 (2023).
[12]J.-W. Chung and F. S. Ohuchi, MRS Proc. **449**, 379 (1996).
[13]P. Gupta *et al.*, Sci. Rep. **6**, 23708 (2016).
[14]S. Li, D. Ouyang, N. Zhang, Y. Zhang, A. Murthy, Y. Li, S. Liu, and T. Zhai, Adv. Mater. **35**, 2211855 (2023).
[15]E. R. Braithwaite and J. Haber, *Molybdenum: An Outline of Its Chemistry and Uses* (Elsevier Science, Amsterdam, 2013).
[16]S. Cadot *et al.*, Nanoscale **9**, 538 (2017).
[17]X. Li and H. Zhu, J. Materiomics **1**, 33 (2015).
[18]D. Jariwala, V. K. Sangwan, L. J. Lauhon, T. J. Marks, and M. C. Hersam, ACS Nano **8**, 1102 (2014).
[19]W.-F. Hsu, L.-S. Lu, P.-C. Kuo, J.-H. Chen, W.-C. Chueh, H. Yeh, H.-L. Kao, J.-S. Chen, and W.-H. Chang, ACS Appl. Nano Mater. **2**, 1964 (2019).
[20]H.-Y. Chien, P.-C. Kuo, H.-L. Kao, J.-S. Chen, M.-R. Chen, L.-S. Lu, W.-C. Chueh, and W.-H. Chang, J. Cryst. Growth **544**, 125726 (2020).
[21]Y. Yin *et al.*, Materials **11**, 2464 (2018).
[22]A. M. Alsaad, Q. M. Al-Bataineh, I. A. Qattan, A. A. Ahmad, A. Ababneh, Z. Albataineh, I. A. Aljarrah, and A. Telfah, Front. Phys. **8**, 115 (2020).
[23]A. Ababneh, A. M. K. Dagamseh, Z. Albataineh, M. Tantawi, Q. M. Al-Bataineh, M. Telfah, T. Zengerle, and H. Seidel, Microsyst. Technol. **27**, 3149 (2021).
[24]S. Cadot, *Élaboration de Monocouches de Dichalcogénures de Métaux de Transition Du Groupe (VI) Par Chimie Organométallique de Surface* (Université de Lyon, Lyon, France, 2017).
[25]A. Koma, K. Sunouchi, and T. Miyajima, Microelectron. Eng. **2**, 129 (1984).
[26]B. Riah, J. Camus, A. Ayad, M. Rammal, R. Zernadji, N. Rouag, and M. A. Djouadi, Coatings **11**, 1063 (2021).
[27]F. Martin, P. Muralt, M.-A. Dubois, and A. Pezous, J. Vac. Sci. Technol. A **22**, 361 (2004).